A two dimensions modeling of non-collocated piezoelectric patches bonded on thin structure

H. Hariri, Y. Bernard, A. Razek

Research Article **Open Access**

H. Hariri*, Y. Bernard, and A. Razek

A two dimensions modeling of non-collocated piezoelectric patches bonded on thin structure

Abstract: The system studied in this paper consists of thin structure with several piezoelectric patches bonded on its surface. The patches are used as actuators and sensors. Based on Kirchhoff-Love hypothesis, linear constitutive relations, plane stress formulation and Hamilton principle, we have developed a 2D model for this system using the finite element method. It is not a standard 2D model, since the calculation is performed on a structure that does not have symmetries that allow such easy assumptions. The originality of the work consists in the use of the concept of neutral plane to model this asymmetric system in 2D. This technique, beside good precision, saves computational time. An experimental device has been also built and tested to validate the model. The structural damping is included in the model to match the damping behavior of the real system. Optimizations of the thickness of piezoelectric patches and materials used in the thin structures are also presented in the paper.

Keywords: Non-collocated piezoelectric patches; thin structure; neutral plane; Hamilton principle; finite element modeling

DOI 10.1515/cls-2015-0002
Received July 15, 2014; accepted November 14, 2014

1 Introduction

Thin structures containing piezoelectric materials are widely used to control vibrations [1–5], for detecting damage in the structure [6–13], to design actuators like inchworm actuators, micropumps, valves, miniature robots, motors, etc. [14–18], to design sensors and for energy harvesting [19–25]. Two large branches are studied in the literature due to their domain of applications, namely beam and plate structures. On the other hand, these systems may be symmetrical or asymmetrical where the piezoelectric materials are collocated or not on the thin beam/plate. In a symmetrical system the piezoelectric materials are bonded face-to-face on both sides of the beam/plate while in an asymmetrical one the piezoelectric materials are bonded only on one side surface of the structure. It may be noted that there is another type of structure containing piezoelectric materials where the piezoelectric materials are embedded in the beam/plate [7], this type of structure is not concerned in this study.

For symmetrical or asymmetrical beam structures with respectively collocated or non-collocated piezoelectric materials, a 1D analytical or numerical model can be used to model such system; examples for modeling symmetrical systems can be found in [2, 26–32] and for asymmetrical ones in [1, 28, 33–35]. In the first case the neutral axis is taken as the symmetry axis (mid plane) of the system while in the case of asymmetrical systems it is necessary to determine such neutral axis.

In the case of plate structures, 2D or 3D Finite Element Method (FEM) can be used to model the system. In the 3D approach volume elements are used while in the 2D case surface elements are used while the 3^{rd} dimension is introduced in the model equations. It is obvious that the second approach is faster but a little more complicated in model formulation.

Several papers in literature are devoted for modeling thin structure with piezoelectric patches using the 2D approach in the case where the symmetry of the system is maintained at the disposal of patches [2, 27, 28, 36–38]. The 2D approach is more difficult for an asymmetrical structure, where piezoelectric patches are not collocated (patches bonded on only one side of structure surface), due to the fact that the neutral plane of the structure is not confused with the mid plane as in the case of a symmetrical structure. This case is not reported yet in the literature and it will be the aim of this paper.

***Corresponding Author: H. Hariri:** Laboratoire de Génie Electrique de Paris (LGEP) / SPEE-Labs, CNRS UMR 8507; SUPELEC; Université Pierre et Marie Curie P6; Université Paris-Sud 11; 11 rue Joliot Curie, Plateau de Moulon F91192 Gif sur Yvette CEDEX, E-mail: haririhas@gmail.com

Y. Bernard, A. Razek: Laboratoire de Génie Electrique de Paris (LGEP) / SPEE-Labs, CNRS UMR 8507; SUPELEC; Université Pierre et Marie Curie P6; Université Paris-Sud 11; 11 rue Joliot Curie, Plateau de Moulon F91192 Gif sur Yvette CEDEX

The aim of this paper is to develop a 2D FEM to model an asymmetrical system where non-collocated piezoelectric patches are bonded on a thin structure, using the variation of the neutral plane and to validate it experimentally. Two cases are treated, the first is the case said ''actuator-sensor" where some patches are used as sensors and others as actuators, while the second is the case of "actuator-actuator", where all patches are used as actuators. First, we present the studied system, the model assumptions, setting equation and variational principle using Hamilton principle. We then present the FEM model of the system and its validation by comparing the results with experiment in the case of a plate structure. The comparison has been done at resonance frequencies and concerned the deformation of the system for an applied voltage to actuator piezoelectric patches, as well as the obtained voltage for sensor piezoelectric patches. After validation of the model, a study of the optimum thickness of piezoelectric patches, which gives a maximum displacement of the structure, is done for several types of structure materials. Also a study of the variation of the resonance frequency depending on the thickness of piezoelectric patches is given, thus allows choosing the optimum thickness of piezoelectric patches and the most suitable materials.

2 Presentation of the studied device

The studied device consists of a thin structure with several piezoelectric patches bonded on one side of its surface i.e. non-collocated piezoelectric patches (asymmetrical system). Examples of such asymmetric systems are shown in Fig. 1 where four colored rectangles stand for piezoelectric patches are bonded on one side of rectangular and circular thin structures with and without holes. As you can see from figure, our studied system is modeled in the plane 2D (x,y) , the third dimension (z) is taken in calculation, thanks to the use of the concept of neutral plane. This allows us to model this asymmetric system in only two dimensions as presented in figure.

3 Variational principle

Several ceramic PZT patches are bonded on one side of the structure and they are polarized along the axis z. Given the geometry of the system where the thickness is very small compared to the other two dimensions, the stress along

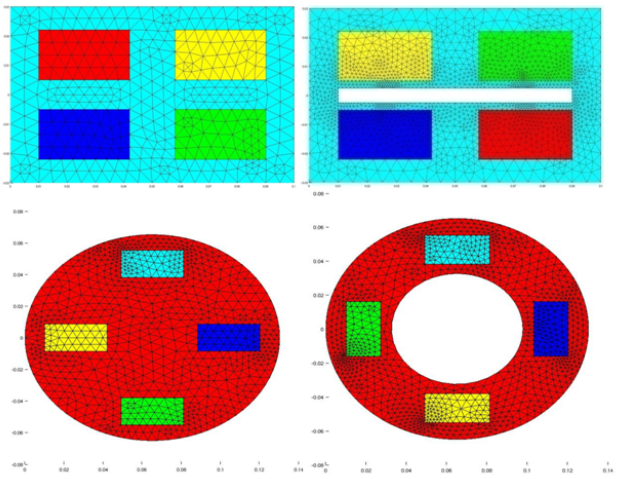

Figure 1: Non-collocated piezoelectric patches bonded on structures.

the z axis is neglected, and therefore plane stress formulation is adopted. The equation of the system is determined based on Kirchhoff-Love hypotheses. Plane stress is assumed in x and y directions. With the assumption of small deformations (deformation less than a fifth of the thickness), the cross-section remains perpendicular to the neutral plane after deformation. The electric field is assumed to be uniformly distributed in the z direction and thus the displacement field becomes

$$\{u\} = \begin{cases} u_1(x,y,z,t) \approx -(z-z_n)\partial_x w(x,y,t) \\ u_2(x,y,z,t) \approx -(z-z_n)\partial_y w(x,y,t) \\ u_3(x,y,z,t) \approx w(x,y,t) \end{cases} \quad (1)$$

Where u_1, u_2 and u_3 are the displacement in x, y and z direction respectively. $w(x,y,t)$ is the displacement along z of the neutral plan (z_n) of the system. The neutral plane (z_n) is a plane in the cross section of the system where there are no longitudinal stresses or strains. It can be determined by using the first Newton law, here z_n is calculated from the bottom of the system according to the coordinate system adopted in Fig. 2, and thus:

$$\iint \sigma_1 dydz = 0 \quad (2)$$

$$\iint \sigma_2 dxdz = 0 \quad (3)$$

Where σ_1 and σ_2 represent respectively the stress in x and y direction. They are obtained using the linear constitutive relations for elastic materials and plane stress formulation. Here we used Voigt notation, that allows us to replace the pairs of letters 11, 22 and 12 by the number 1, 2 and 6, where $2\varepsilon_{12} = \varepsilon_6$ is engineering shear strain.

Under the assumption of linear elastic materials and plane stress formulation, we can write

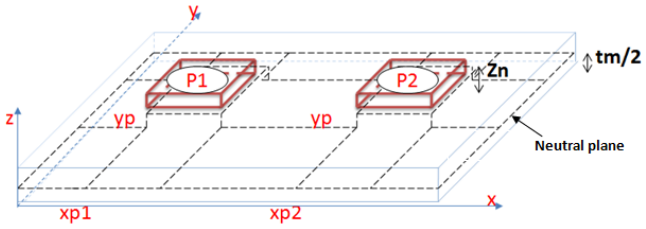

Figure 2: Description of the neutral plane.

$$\begin{pmatrix} \sigma_1^m \\ \sigma_2^m \\ \sigma_6^m \end{pmatrix} = \frac{E_m}{1-\nu_m^2} \begin{bmatrix} 1 & \nu_m & 0 \\ \nu_m & 1 & 0 \\ 0 & 0 & \frac{1-\nu_m}{2} \end{bmatrix} \begin{pmatrix} \varepsilon_1 \\ \varepsilon_2 \\ \varepsilon_6 \end{pmatrix} = \begin{bmatrix} c_{11}^m & c_{12}^m & 0 \\ c_{12}^m & c_{11}^m & 0 \\ 0 & 0 & c_6^m \end{bmatrix} \begin{pmatrix} \varepsilon_1 \\ \varepsilon_2 \\ \varepsilon_6 \end{pmatrix} \tag{4}$$
$$\{\sigma^m\} = [c^m]\{\varepsilon\}$$

$$\begin{pmatrix} \sigma_1^p \\ \sigma_2^p \\ \sigma_6^p \\ D_3 \end{pmatrix} = \begin{bmatrix} \frac{s_{11}^E}{s_{11}^{2E}-s_{12}^{2E}} & \frac{-s_{12}^E}{s_{11}^{2E}-s_{12}^{2E}} & 0 & -\frac{d_{31}}{s_{11}^E+s_{12}^E} \\ \frac{-s_{12}^E}{s_{11}^{2E}-s_{12}^{2E}} & \frac{s_{11}^E}{s_{11}^{2E}-s_{12}^{2E}} & 0 & -\frac{d_{31}}{s_{11}^E+s_{12}^E} \\ 0 & 0 & \frac{1}{2\times 2\left(s_{11}^E-s_{12}^E\right)} & 0 \\ \frac{d_{31}}{s_{11}^E+s_{12}^E} & \frac{d_{31}}{s_{11}^E+s_{12}^E} & 0 & \varepsilon_{33}^\sigma - 2\frac{d_{31}^2}{s_{11}^E+s_{12}^E} \end{bmatrix} \begin{pmatrix} \varepsilon_1 \\ \varepsilon_2 \\ \varepsilon_6 \\ E_3 \end{pmatrix} =$$
$$= \begin{bmatrix} c_{11}^p & c_{12}^p & 0 & -e_{31}^p \\ c_{12}^p & c_{11}^p & 0 & -e_{32}^p \\ 0 & 0 & c_6^p & 0 \\ e_{31}^p & e_{32}^p & 0 & \epsilon_p^\varepsilon \end{bmatrix} \begin{pmatrix} \varepsilon_1 \\ \varepsilon_2 \\ \varepsilon_6 \\ E_3 \end{pmatrix} \tag{5}$$
$$\begin{Bmatrix} \sigma^p \\ D \end{Bmatrix} = \begin{bmatrix} [c^p] & -\{e\}^t \\ \{e\} & \{\epsilon_p^\varepsilon\} \end{bmatrix} \begin{Bmatrix} \varepsilon \\ E \end{Bmatrix}$$

$$\text{with } \{\varepsilon\} = \begin{pmatrix} \varepsilon_1 \\ \varepsilon_2 \\ \varepsilon_6 \end{pmatrix} = \begin{pmatrix} \partial_x u_1 \\ \partial_y u_2 \\ \partial_y u_1 + \partial_x u_2 \end{pmatrix} = \begin{pmatrix} -(z-z_n)\,\partial^2{}_x w(x,\,y,\,t) \\ -(z-z_n)\,\partial^2{}_y w(x,\,y,\,t) \\ -2(z-z_n)\partial^2_{xy} w(x,\,y,\,t) \end{pmatrix} \tag{6}$$

where σ_1^m and σ_1^p are the axial stresses along x direction for the elastic structure and piezoelectric patches respectively, σ_2^m and σ_2^p are the axial stresses along y direction for the elastic structure and piezoelectric patches respectively, σ_6^m and σ_6^p are the shear stresses in the plane (x, y) for the elastic structure and piezoelectric patches respectively. E_m and ν_m are the Young's modulus and Poisson's ratio for the elastic structure. $\varepsilon_1$and ε_2 are the axial strains along x and y direction respectively. ε_6 is the shear strain in the plane (x, y). s_{11}^E, s_{12}^E and d_{31} are the elastic compliances and piezoelectric coefficient for the piezoelectric patches and ε_{33}^σ is the dielectric permittivity at constant stress. Noted by l_p, l_m, b_p, b_m, t_p, t_m the length, width and thickness for the piezoelectric patches and the thin structure respectively. The neutral plane is at the mid plane of the thin structure when there are no piezoelectric patches on it. In the case where they bonded it at the surface of the thin structure, the neutral plane is determined by integrating the equations 2 and 3 and we obtain:

$$\int_b \int_p \partial^2{}_x w\, dy \left[\int_t \int_p {c_{11}}^p (z - z_n)\, dz + \int_t \int_m {c_{11}}^m (z - z_n)\, dz \right] +$$
$$\int_b \int_p \partial^2{}_y w\, dy \left[\int_t \int_p {c_{12}}^p (z - z_n)\, dz + \int_t \int_m {c_{12}}^m (z - z_n)\, dz \right] = 0 \tag{7}$$

$$\int_l \int_p \partial^2{}_x w\, dx \left[\int_t \int_p {c_{12}}^p (z - z_n)\, dz + \int_t \int_m {c_{12}}^m (z - z_n)\, dz \right] +$$
$$\int_l \int_p \partial^2{}_y w\, dx \left[\int_t \int_p {c_{11}}^p (z - z_n)\, dz + \int_t \int_m {c_{11}}^m (z - z_n)\, dz \right] = 0 \tag{8}$$

Equations 7 and 8 give

$$\int_t \int_p {c_{11}}^p (z - z_n)\, dz + \int_t \int_m {c_{11}}^m (z - z_n)\, dz =$$
$$\int_t \int_p {c_{12}}^p (z - z_n)\, dz + \int_t \int_m {c_{12}}^m (z - z_n)\, dz \tag{9}$$

And after simplification, the neutral plane z_n calculated from the bottom of the system according to the coordinate system adopted in Fig. 3 is equal to

$$\begin{cases} = \dfrac{1}{2} \dfrac{(c_{11}^m - c_{12}^m) t_m^2 + (c_{11}^p - c_{12}^p) t_p^2 + 2(c_{11}^p - c_{12}^p) t_p t_m}{(c_{11}^m - c_{12}^m) t_m + (c_{11}^p - c_{12}^p) t_p} \\ \text{if } (x,\ y) \in \text{to the piezoelectric pathes} \\ = \dfrac{t_m}{2} \quad \text{if not} \end{cases} \tag{10}$$

The discontinuity on the neutral plan is already reported on [17] using an analytical method in the case of a beam with one piezoelectric patch bonded on it. This discontinuity allows us to model this asymmetric system in two dimensions and it will be validated experimentally in this paper.

Applying Hamilton principle as described in [1], we obtain the variational equation that represents the mechanical and piezoelectric system.

$$\int_V (-\rho\{\delta u\}^t\{\ddot{u}\} - \{\delta\varepsilon\}^t[c]\{\varepsilon\} + \{\delta\varepsilon\}^t[e]^t\{E\} +$$
$$\{\delta E\}^t[e]\{\varepsilon\} + \{\delta E\}^t[\epsilon^\varepsilon]\{E\} + \{\delta u\}^t\{F_v\})dV +$$
$$t_p\{\delta E\}Q = 0 \tag{11}$$

where ρ and $[c]$ are volume density and stiffness matrix for both thin structure and piezoelectric patches.

Kirchhoff-Love plate theory is used because we are considering the case of thin structure with non-collocated piezoelectric patches; in the case of thick structure more precise theory such as Mindlin-Reissner theory [2, 39] should be considered taking into account this variation of the neutral plane in the case of asymmetric system.

4 Modeling of the system using 2D FEM

In a finite element formulation, the unknowns are the values of the solution to the nodes of the mesh.

The displacement field $\{u\}$ is related to the values of the corresponding node $\{u_i\}$ by the interpolation functions. Lagrangian functions are not used in this problem because the solution w (x, y, t) must be C^1-continuous while Lagrange only provides C^0 continuity. The choice of Hermit elements satisfies this condition. Thus, with the Hermit elements, the solution $\{u\}$ which depends only on w (x, y, t) in this case reads as follows on a triangle i:

$$w(x, y, t) = [\lambda(x,\ y)]\{U_i\} \tag{12}$$

where $[\lambda(x,\ y)] = [\lambda_1, \lambda_2, \ldots, \lambda_9]$ are the interpolation functions [40], and $\{U_i\} = \begin{bmatrix} w_i \\ \partial_x w_i \\ \partial_y w_i \\ w_{i+1} \\ \partial_x w_{i+1} \\ \partial_y w_{i+1} \\ w_{i+2} \\ \partial_x w_{i+2} \\ \partial_y w_{i+2} \end{bmatrix}$ are the unknowns of the triangle i.

Integrating equation 11 over the entire volume of the system, we obtain an equation that describes the system by surface integrals along x and y. Integration of this equation in the plane (x, y) of the system returns to integrate on each triangle and make the sum. The boundary conditions are taken into account in the assembly of matrices and the numerical equation is then written taking into account the damping matrix as follows

$$\begin{bmatrix} [M_{mm}] & 0 \\ 0 & 0 \end{bmatrix} \begin{bmatrix} \{\ddot{U}_i\} \\ \{\ddot{E}_{3pj}\} \end{bmatrix} +$$
$$\begin{bmatrix} [C_{mm}] & 0 \\ 0 & 0 \end{bmatrix} \begin{bmatrix} \{\dot{U}_i\} \\ \{\dot{E}_{3pj}\} \end{bmatrix} +$$
$$\begin{bmatrix} [K_{mm}] & [K_{mvpj}] \\ [K_{vmpj}] & [K_{vvpj}] \end{bmatrix} \begin{bmatrix} \{U_i\} \\ \{E_{3pj}\} \end{bmatrix} = \begin{bmatrix} \{F_i\} \\ t_p\{Q_{pj}\} \end{bmatrix} \tag{13}$$

with:
$[M_{mm}]$: the structural mass matrix
$[C_{mm}]$: the structural damping matrix
$[K_{mm}]$: the structural stiffness matrix
$[K_{mvpj}]$ and $[K_{vmpj}] = [K_{mvpj}]^t$: the piezoelectric stiffness matrices for n piezoelectric patches
$[K_{vvpj}]$: the dielectric stiffness matrix for n piezoelectric patches
$\{U_i\}$: the vector with nodal structural displacements
$\{E_{3pj}$: the vector with the electric fields for the n piezoelectric patches
F_i: the vector with nodal forces
$\{Q_{pj}\}$: the vector with nodal charges for n piezoelectric patches
where:
$[K_{mvpj}] = \begin{bmatrix} K_{mvp1} & \cdots & K_{mvpn} \end{bmatrix}$

$[K_{vvpj}]$ is a diagonal matrix and it is equal to $\begin{bmatrix} K_{vvp1} & 0 & \cdots & 0 \\ 0 & \ddots & 0 & \vdots \\ \vdots & 0 & \ddots & 0 \\ 0 & \cdots & 0 & K_{vvpn} \end{bmatrix}$

We should know that the damping matrix $[C_{mm}]$ is added to the system and it is determined experimentally to match the damping behavior of the real system.

Particular cases for two and four piezoelectric patches are taken in appendix.

4.1 Actuator-sensor

The first case treated is the case actuator-sensor where the patches actuators are deformed under the effect of an electric fields $E_{3pa}(t)$ and the patches sensors behave like an open circuit ($Q_{ps} = 0$), while no external loads applied. The letter 'a' is referred to actuators patches and the letter 's' to sensors patches. The equation 13 becomes:

$$\begin{bmatrix} [M_{mm}] & 0 & 0 \\ 0 & 0 & 0 \\ 0 & 0 & 0 \end{bmatrix} \begin{bmatrix} \{\ddot{U}_i\} \\ t_p\{\ddot{Q}_{pa}\} \\ \{\ddot{E}_{3ps}\} \end{bmatrix} + \begin{bmatrix} [C_{mm}] & 0 & 0 \\ 0 & 0 & 0 \\ 0 & 0 & 0 \end{bmatrix} \begin{bmatrix} \{\dot{U}_i\} \\ t_p\{\dot{Q}_{pa}\} \\ \{\dot{E}_{3ps}\} \end{bmatrix} + \begin{bmatrix} [K_{mm} - \sum_{j \in a} K_{mvpj} K_{vvpj}^{-1} K_{vmpj}] & \cdots & [K_{mvpa} K_{vvpa}^{-1}] & [K_{mvps}] \\ -[K_{vvpa}^{-1} K_{vmpa}] & \cdots & [K_{vvpa}^{-1}] & 0 \\ [K_{vmps}] & & 0 & [K_{vvps}] \end{bmatrix} \begin{bmatrix} \{U_i\} \\ t_p\{Q_{pa}\} \\ \{E_{3ps}\} \end{bmatrix} = \begin{bmatrix} 0 \\ \{E_{3pa}\} \\ 0 \end{bmatrix} \tag{14}$$

To clarify, a particular case of four piezoelectric patches where two patches are considered as actuators and the two others as sensors is taken in Appendix.

4.2 Actuator- actuator

In this case all patches are used as actuators while no external loads applied. The model system obtained from equation 13 is governed by the following matrix equation

$$\begin{bmatrix} [M_{mm}] & 0 \\ 0 & 0 \end{bmatrix} \begin{bmatrix} \{\ddot{U}_i\} \\ t_p\{\ddot{Q}_{pa}\} \end{bmatrix} + \begin{bmatrix} [C_{mm}] & 0 \\ 0 & 0 \end{bmatrix} \begin{bmatrix} \{\dot{U}_i\} \\ t_p\{\dot{Q}_{pa}\} \end{bmatrix} + \begin{bmatrix} [K_{mm} - \sum_{j \in a} K_{mvpj} K_{vvpj}^{-1} K_{vmpj}] & \cdots \\ -[K_{vvpa}^{-1} K_{vmpa}] & \\ \cdots & [K_{mvpa} K_{vvpa}^{-1}] \\ & [K_{vvpa}^{-1}] \end{bmatrix} \begin{bmatrix} \{U_i\} \\ t_p\{Q_{pa}\} \end{bmatrix} = \begin{bmatrix} 0 \\ \{E_{3pa}\} \end{bmatrix} \tag{15}$$

A particular case of four piezoelectric patches is taken in Appendix to clarify.

5 Model validation

To validate our model experimentally, we took an aluminum plate structure fixed at one end, the other being left free. Two ceramic PZT patches are bonded on one side of the plate and they are polarized along the axis z. Properties and geometrical parameters for the piezoelectric ceramic PZT and the elastic structure are presented in Table 1 and the system is shown in Fig. 3. We begin the process of model validation by comparing the non-damping resonant frequencies of the model with the experimental ones, then we apply a sinusoidal electrical voltage to one patch, we measure the transverse displacement of the plate and the obtained electrical voltage for the other patch in the case of open circuit and resistance shunt circuit. All measures are done using a high resolution laser interferometer LK-G3001PV Keyence France.

The damping matrix [C] is determined experimentally. The Rayleigh damping is considered as a classical way to model the damping of the structure. It uses the assumption that the damping matrix is proportional to a linear combination of the mass matrix and the stiffness [41, 42].

$$[C_{mm}] = \alpha[M_{mm}] + \beta[K_{mm}] \tag{16}$$

α and β are the Rayleigh coefficients.

In the formulation of equation 16, orthogonal transformation form the following equation [41],

$$2\varepsilon_i w_i = \alpha + \beta w_i^2 \tag{17}$$

where ε_i is the damping ratio and w_i is the resonance frequency.

It can be seen from 17 that, by experimentally obtaining the damping ratio ε_i for two different resonant modes, the Rayleigh coefficients α and β can be calculated. The experimental damping ratios corresponding of two vibration modes were obtained from the system resonance curve [42]. The resulting Rayleigh coefficients and damping ratio are given in table 2.

Table 1: Properties and geometry of the system

	PZT (p)	Elastic structure (m)
Young's modulus ($N.m^{-2}$)	/	$E_m = 69\times10^9$
Poison's ratio	/	$\upsilon_m = 0.33$
Volume density ($Kg.m^{-3}$)	$\rho_p = 7900$	$\rho_m = 2700$
Relative permittivity	$\varepsilon_{33r} = 1282$	/
Piezoelectric constant ($m.V^{-1}$)	$d_{31} = -1.3\times 10^{-10}$	/
Elastic compliances (Pa^{-1})	$S_{11} = 1.3 \times 10^{-11}$ $S_{12} =$ -4.76×10^{-12}	/
Max peak to peak electric field($V.mm^{-1}$)	$E_{max} = 300$	/
Max compressive strength (Pa)	$\sigma_{max} = 600 \times 10^6$	/
Length × width × thickness (mm^3) $(l_p, l_m) \times (b_p, b_m) \times (t_p, t_m)$	32×17 ×0.27	100 × 60 × 0.5
X_{p1}, X_{p2}, y_p (mm)	10,58, 21.5	/

Table 2: Experimental determination of damping parameters

Rayleigh coefficients	α	β
	1.7706	4.1158e-06

5.1 Resonance frequencies comparison

In short-circuit, the voltage E_{3p} is zero. In the case of an open circuit, the electric charge Q_p is zero. The resonance frequencies and modes shapes of the system when the two electrodes of the piezoelectric patches are short circuited ($E_{3p} = 0$) are given by

$$([K_{mm}] - (2\pi f_n)^2 [M_{mm}])\{U\} = 0 \tag{18}$$

Fig. 4 shows the first fifteen resonant frequencies determined experimentally and by finite element modeling. The figure shows a good agreement between model and experimental measurements. Modes shapes for the first six resonant frequencies are given in Fig. 5.

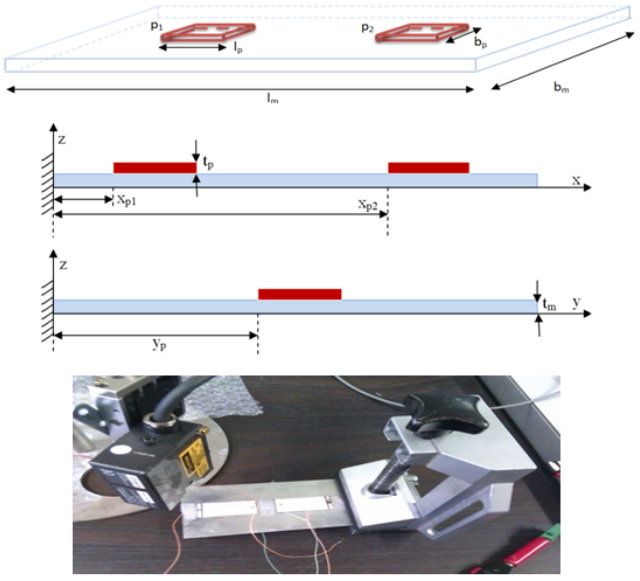

Figure 3: Studied device.

Mode	FE code (2D)	Experimental
1	48.22	43.5
2	197.84	190
3	300.28	271
4	653.27	629
5	841.02	905
6	1072.7	951
7	1240.8	1132
8	1337.9	1332
9	1814.6	1676
10	1906.8	1855
11	2029.6	1952
12	2470.2	2122
13	2604.8	2602
14	2778.6	2750
15	2958.2	2817

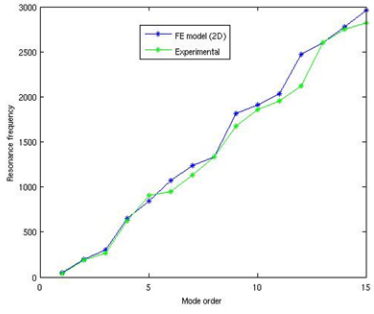

Figure 4: Resonance frequencies comparison in Hz.

5.2 Transverse displacements comparison

We treat here the case sensor-actuator where the actuator is powered by a sinusoidal voltage of 20V amplitude and frequency equal successively to the first, second and fourth resonant frequency of the system. Measurements of displacement along the z axis are performed on a portion of the device (Fig. 6) and they are compared with the model results given by the following equation

$$\left[-(2\pi f_n)^2\begin{bmatrix} M & 0 & 0 \\ 0 & 0 & 0 \\ 0 & 0 & 0 \end{bmatrix} + \mathrm{j}(2\pi f_n)\begin{bmatrix} C & 0 & 0 \\ 0 & 0 & 0 \\ 0 & 0 & 0 \end{bmatrix} + \begin{bmatrix} K_{mm} - K_{mvp2}K_{vvp2}^{-1}K_{vmp2} & K_{mvp1} & \cdots \\ K_{vmp1} & K_{vvp1} & \cdots \\ -K_{vvp2}^{-1}K_{vmp2} & 0 & \end{bmatrix} \begin{bmatrix} K_{mvp2}K_{vvp2}^{-1} \\ 0 \\ K_{vvp2}^{-1} \end{bmatrix}\right] \begin{bmatrix} U_i \\ E_{3p1} \\ t_p Q_{p2} \end{bmatrix} = \begin{bmatrix} 0 \\ 0 \\ E_{3p2} \end{bmatrix} \tag{19}$$

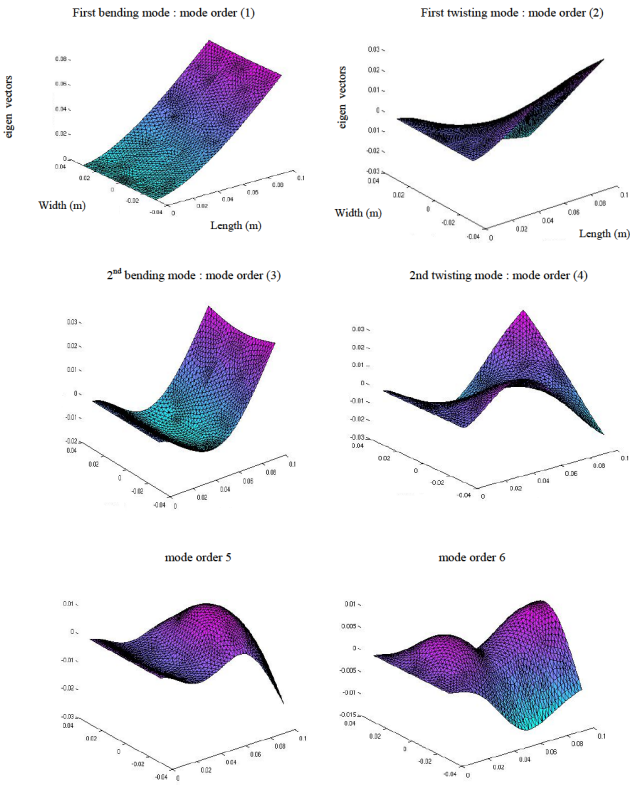

Figure 5: Modes shapes of the system

Figure 7 shows displacements comparison between experimental measurements and simulation results.

5.3 Piezoelectric sensor

As we said in the section 5.2, we treat here the sensor-actuator case where the patch powered by a sinusoidal voltage of 20 V amplitude is called piezoelectric actuator and the other is called piezoelectric sensor, as shown Fig. 8. After comparing the actuator functionality of the model by measuring the transverse displacement of the system, we are comparing the sensor functionality by

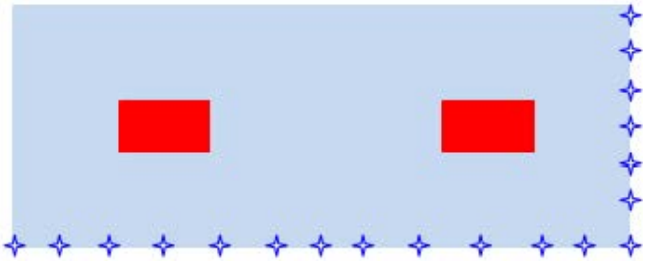

Figure 6: Experimental measurements points.

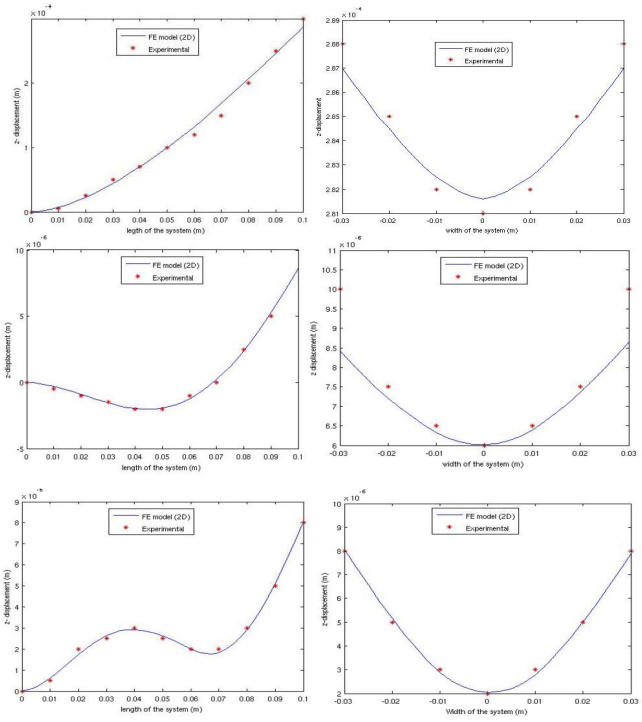

Figure 7: Transverse displacements comparison for the first, second and fourth resonance frequency

measuring the obtained voltage for the piezoelectric sensor in the case of open circuit and shunt resistance circuit (50 kΩ). The resistance is added to the damping matrix as demonstrated Hariri et al. in [1] and results for the two cases are illustrated in table 3.

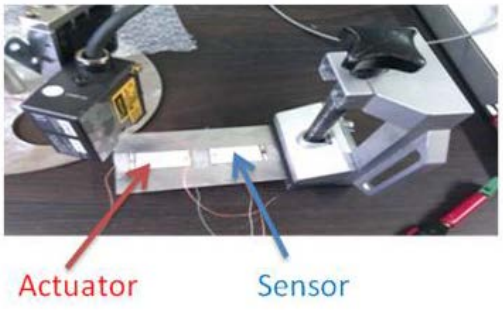

Figure 8: Actuator-sensor functionality.

6 Optimal design

In this section, we will study the influence of the thickness of the piezoelectric patches and the material rigidity of the structure on the amplitude of the transverse displacement and the resonance frequency of the system. We are interested in the thickness which gives a maximum transverse displacement of the plate and this optimal thickness is the same for static and dynamic operation of the system [43]. A static study is done to determine this thickness. The optimum thickness for the two patches is determined for a constant electric field applied to a patch, while the other being kept in open circuit. By varying the thickness of the patches and calculating the transverse displacement at a given point for different rigidities of the plate (table 4), we obtain the curves of Fig. 9. The decrease (in each curve) in Fig. 9 shows that when the thickness of the piezoelectric patches becomes large, the bending stiffness of the system becomes more important than the bending moment generated by piezoelectric patches [44]. We can also see the influence of the stiffness of the structure, on transverse displacement function of piezoelectric thickness. Fig. 10 represents the first resonant frequency depending on the thickness of piezoelectric patches. We are interested at the material that gives the best compromise between maximum transverse displacement and maximum frequency. According to figure 9 & 10, we get the aluminum as the better elastic materials. For this type of materials we can note that the optimal piezoelectric thickness is equal to 0.45 mm compared to 0.5 mm thickness of the plate as shown in table 1. When we are interested in maximum energy conversion from electrical to mechanical, in the case of an aluminum elastic material for example the maximum displacement is obtained at 0.45 mm and in the case of steel at 0.72 mm thickness of piezoelectric patches compared to 0.5 mm thickness of the plate.

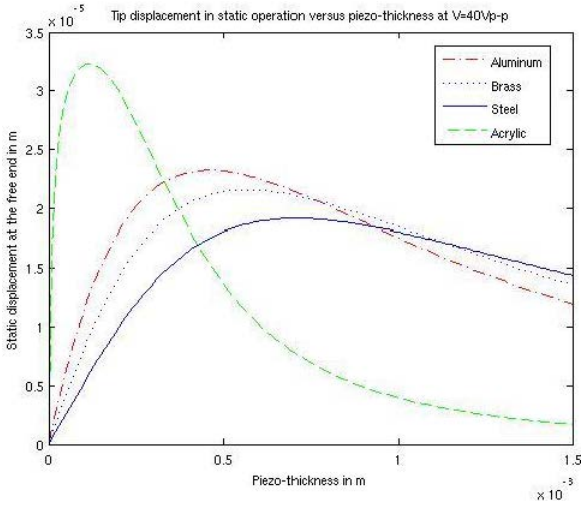

Figure 9: Displacements at the free end of the system depending on the thickness of piezoelectric patches.

Table 3: Obtained voltage for the piezoelectric sensor.

Frequency	*Open circuit*		*Resistance shunt circuit*	
	Experimental	*2D FE model*	*Experimental*	*2D FE model*
f1	2 V	2.1 V	0.5 V	0.53 V
f3	4 V	4.1 V	3.4 V	3.41 V
f5	14.5 V	14.2 V	12.5 V	12.9 V
f10	29 V	29.05 V	28.8 V	28.8 V
f14	12 V	12.09 V	11.8 V	

Table 4: Materials properties used for the elastic structure.

Materials	*Young's modulus* N/m^2	*Density* Kg/m^3	*Poisson's ratio*
Aluminum	69×10^9	2700	0.33
Brass	11×10^{10}	8800	0.35
Steel	19.5×10^{10}	7700	0.3
Acrylic	0.31×10^{10}	1185	0.4

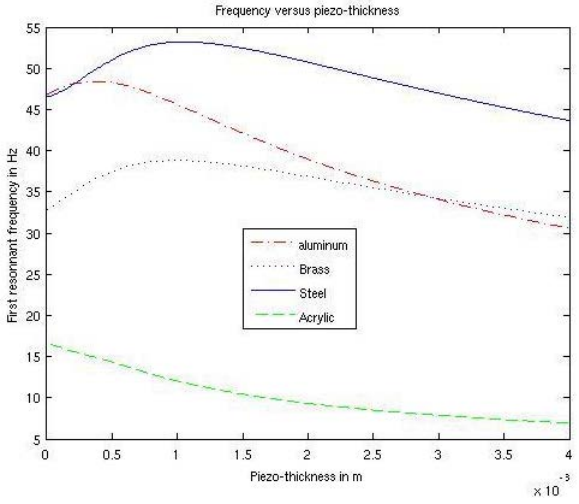

Figure 10: First resonant frequency depending on the thickness of piezoelectric patches.

7 Conclusions

In this article, we have developed a finite element model for an asymmetrical system taking into consideration the variation of the neutral plan of the system. The system consists of an elastic thin structure with piezoelectric patches bonded on its surface. Using the notion of the neutral plane in our asymmetrical system allows us to model it in two dimensions, taking into account the third dimension in the analysis. This saves computing time compared to a three-dimensional simulation because of 2D instead 3D simulation. We have seen also, that in analyzing the maximum displacement of the system, the optimal piezoelectric thickness could be comparable to the thickness of the elastic structure. The model can also optimize the position of patches based on the intended applications. Special damping techniques can be analyzed with the help of the developed model when connecting electrical circuits in the system. This asymmetrical system can be used to detect damage on the structure, to reduce unnecessary vibrations, as well as for robotic applications. In all these applications the proposed method is more practical due to computation time saving.

Nomenclature

$\{\}^t$ *transposed vector*
$\{u\}$ *displacement vector*
$\{\delta u\}$ *variation of u*
$\{\dot{u}\}$ *first derivative with respect to time*
$\{\ddot{u}\}$ *second derivative with respect to time*
u_i *displacement in i direction*
$w(x, y, t)$ *transverse deflection*
$\partial_i w$ *or* $\frac{\partial w}{\partial i}$ *first derivative with respect to i*
$\partial_i^2 w$ *or* $\frac{\partial^2 w}{\partial i^2}$ *second derivative with respect to i*
z_n *neutral plane*
σ_i^m *stress in i direction for the elastic structure*
σ_i^p *stress in i direction for the piezoelectric patch*

E_m *Young′s modulus for the elastic structure*
ν_m *Poisson′s ratio for the elastic structure*
ε_i *strain in i direction*
s_{11}^E, s_{12}^E *elastic compliances*
$(l_p, l_m, b_p, b_m, t_p, t_m)$ *length, width and thickness for the piezoelectric patch and the thin structure respectively*
ρ *volume density*
σ^m *stress vector for the elastic structure*
c^m *stiffness matrix for the elastic structure*
ε *strain vector*
σ^p *stress vector for the piezoelectric patch*
c^p *stiffness matrix for the piezoelectric patch*
e *piezoelectric constant vector*
ϵ_p^ε *piezoelectric permittivity at constant strain*
E *electric field vector*
D *electric displacement vector*
F_v *body applied forcesdV volume element*

Appendix: Particular cases

1. Modeling of the system using 2D FEM In the case of two piezoelectric patches, the equation 13 wrote as:

$$\begin{bmatrix} M_{mm} & 0 & 0 \\ 0 & 0 & 0 \\ 0 & 0 & 0 \end{bmatrix} \begin{bmatrix} \ddot{U}_i \\ \ddot{E}_{3p1} \\ \ddot{E}_{3p2} \end{bmatrix} + \begin{bmatrix} C_{mm} & 0 & 0 \\ 0 & 0 & 0 \\ 0 & 0 & 0 \end{bmatrix} \begin{bmatrix} \dot{U}_i \\ \dot{E}_{3p1} \\ \dot{E}_{3p2} \end{bmatrix} + \begin{bmatrix} K_{mm} & K_{mvp1} & K_{mvp2} \\ K_{vmp1} & K_{vvp1} & 0 \\ K_{vmp2} & 0 & K_{vvp2} \end{bmatrix} \begin{bmatrix} U_i \\ E_{3p1} \\ E_{3p2} \end{bmatrix} = \begin{bmatrix} F_i \\ t_p Q_{p1} \\ t_p Q_{p2} \end{bmatrix} \tag{20}$$

In the case of two piezoelectric patches, the equation 13 wrote as:

$$\begin{bmatrix} M_{mm} & 0 & 0 & 0 & 0 \\ 0 & 0 & 0 & 0 & 0 \\ 0 & 0 & 0 & 0 & 0 \\ 0 & 0 & 0 & 0 & 0 \\ 0 & 0 & 0 & 0 & 0 \end{bmatrix} \begin{bmatrix} \ddot{U}_i \\ \ddot{E}_{3p1} \\ \ddot{E}_{3p2} \\ \ddot{E}_{3p3} \\ \ddot{E}_{3p4} \end{bmatrix} + \begin{bmatrix} C_{mm} & 0 & 0 & 0 & 0 \\ 0 & 0 & 0 & 0 & 0 \\ 0 & 0 & 0 & 0 & 0 \\ 0 & 0 & 0 & 0 & 0 \\ 0 & 0 & 0 & 0 & 0 \end{bmatrix} \begin{bmatrix} \dot{U}_i \\ \dot{E}_{3p1} \\ \dot{E}_{3p2} \\ \dot{E}_{3p3} \\ \dot{E}_{3p4} \end{bmatrix} + \\ + \begin{bmatrix} K_{mm} & K_{mvp1} & K_{mvp2} & K_{mvp3} & K_{mvp4} \\ K_{vmp1} & K_{vvp1} & 0 & 0 & 0 \\ K_{vmp2} & 0 & K_{vvp2} & 0 & 0 \\ K_{vmp3} & 0 & 0 & K_{vvp3} & 0 \\ K_{vmp4} & 0 & 0 & 0 & K_{vvp4} \end{bmatrix} \begin{bmatrix} U_i \\ E_{3p1} \\ E_{3p2} \\ E_{3p3} \\ E_{3p4} \end{bmatrix} = \begin{bmatrix} F_i \\ t_p Q_{p1} \\ t_p Q_{p2} \\ t_p Q_{p3} \\ t_p Q_{p4} \end{bmatrix} \tag{21}$$

2. Actuator-sensor

Taking the case of four piezoelectric patches where the patch 1 and 3 are considered as actuators while the two others as sensors, the equation 14 is written as:

$$\begin{bmatrix} M_{mm} & 0 & 0 & 0 & 0 \\ 0 & 0 & 0 & 0 & 0 \\ 0 & 0 & 0 & 0 & 0 \\ 0 & 0 & 0 & 0 & 0 \\ 0 & 0 & 0 & 0 & 0 \end{bmatrix} \begin{bmatrix} \ddot{U}_i \\ t_p\ddot{Q}_{p1} \\ t_p\ddot{Q}_{p3} \\ \ddot{E}_{3p2} \\ \ddot{E}_{3p4} \end{bmatrix} + \begin{bmatrix} C_{mm} & 0 & 0 & 0 & 0 \\ 0 & 0 & 0 & 0 & 0 \\ 0 & 0 & 0 & 0 & 0 \\ 0 & 0 & 0 & 0 & 0 \\ 0 & 0 & 0 & 0 & 0 \end{bmatrix} \begin{bmatrix} \dot{U}_i \\ t_p\dot{Q}_{p1} \\ t_p\dot{Q}_{p3} \\ \dot{E}_{3p2} \\ \dot{E}_{3p4} \end{bmatrix} +$$

$$+ \begin{bmatrix} K_{mm} - K_{mvp1}K_{vvp1}^{-1}K_{vmp1} - K_{mvp3}K_{vvp3}^{-1}K_{vmp3} & & K_{mvp1}K_{vvp1}^{-1} & K_{mvp3}K_{vvp3}^{-1} & K_{mvp2} & K_{mvp4} \\ -K_{vvp1}^{-1}K_{vmp1} & & K_{vvp1}^{-1} & 0 & 0 & 0 \\ -K_{vvp3}^{-1}K_{vmp3} & \cdots & 0 & K_{vvp3}^{-1} & 0 & 0 \\ K_{vmp2} & & 0 & 0 & K_{vvp2} & 0 \\ K_{vmp4} & & 0 & 0 & 0 & K_{vvp4} \end{bmatrix} \cdots \begin{bmatrix} U_i \\ t_pQ_{p1} \\ t_pQ_{p3} \\ E_{3p2} \\ E_{3p4} \end{bmatrix} =$$

$$= \begin{bmatrix} 0 \\ E_{3p1} \\ E_{3p3} \\ 0 \\ 0 \end{bmatrix}$$

3. Actuator-actuator

Consider the case where four piezoelectric patches are used as actuators, the equation 15 should be written as:

$$\begin{bmatrix} M_{mm} & 0 & 0 & 0 & 0 \\ 0 & 0 & 0 & 0 & 0 \\ 0 & 0 & 0 & 0 & 0 \\ 0 & 0 & 0 & 0 & 0 \\ 0 & 0 & 0 & 0 & 0 \end{bmatrix} \begin{bmatrix} \ddot{U}_i \\ t_p\ddot{Q}_{p1} \\ t_p\ddot{Q}_{p2} \\ t_p\ddot{Q}_{p3} \\ t_p\ddot{Q}_{p4} \end{bmatrix} + \begin{bmatrix} C_{mm} & 0 & 0 & 0 & 0 \\ 0 & 0 & 0 & 0 & 0 \\ 0 & 0 & 0 & 0 & 0 \\ 0 & 0 & 0 & 0 & 0 \\ 0 & 0 & 0 & 0 & 0 \end{bmatrix} \begin{bmatrix} \dot{U}_i \\ t_p\dot{Q}_{p1} \\ t_p\dot{Q}_{p2} \\ t_p\dot{Q}_{p3} \\ t_p\dot{Q}_{p4} \end{bmatrix} +$$

$$+ \begin{bmatrix} K_{mm} - \sum_{a=1}^{4} K_{mvpa}K_{vvpa}^{-1}K_{vmpa} & K_{mvp1}K_{vvp1}^{-1} & & K_{mvp2}K_{vvp2}^{-1} & K_{mvp3}K_{vvp3}^{-1} & K_{mvp4}K_{vvp4}^{-1} \\ -K_{vvp1}^{-1}K_{vmp1} & K_{vvp1}^{-1} & & 0 & 0 & 0 \\ -K_{vvp2}^{-1}K_{vmp2} & 0 & \cdots & K_{vvp2}^{-1} & 0 & 0 \\ -K_{vvp3}^{-1}K_{vmp3} & 0 & & 0 & K_{vvp3}^{-1} & 0 \\ -K_{vvp4}^{-1}K_{vmp4} & 0 & & 0 & 0 & K_{vvp4}^{-1} \end{bmatrix} \cdots \begin{bmatrix} U_i \\ E_{3p1} \\ E_{3p2} \\ E_{3p3} \\ E_{3p4} \end{bmatrix} =$$

$$= \begin{bmatrix} 0 \\ E_{3p1} \\ E_{3p2} \\ E_{3p3} \\ E_{3p4} \end{bmatrix}$$

References

[1] Hariri H., Bernard Y., Razek A., Finite element model of a beam structure with piezoelectric, patches using RL shunt circuits, AC2011, 14th International Conference on active systems for dynamics markets, Darmstadt, Germany, 07-08 September 2011,pp.124-131.

[2] Yasin M. Y., Ahmad N., Alam M. N., Finite element analysis of actively controlled smart plate with patched actuators and sensors, Latin American Journal of Solids and Structures, Vol 7, No 3 (2010) 227-247.

[3] Sharma A., Kumar R., Vaish R., Chauhan V., Lead-free piezoelectric materials' performance in structural active vibration control, Journal of Intelligent Material Systems and Structures, September 2014 vol. 25 no. 13 1596-1604.

[4] Zhang J., He L., Wang E., Active Vibration Control of Piezoelectric Intelligent Structures, Journal of Computers, 03/2010.

[5] Rodriguez-Fortun J. M., Orus J., Alfonso J., Gimeno F. B., Castellanos J. A., Mechatronics, IEEE/ASME Transactions on, Volume: 18, Issue: 1 (2013), pp. 221-229.

[6] Qu G.M., Li Y.Y., Cheng L., Wang B., Analysis of a piezoelectric composite plate with cracks, Journal of composite structures, vol. 72, n°1 (2006) 111-118.

[7] Yan Y.J., Yam L.H., Online detection of crack damage in composite plates using embedded piezoelectric actuators/sensors and wavelet analysis, Journal of Composite Structures, Vol 58, Issue 1 (2002) 29-38.

[8] Jinsong Z., Change G., Likun H., Piezoelectric-based Crack Detection Techniques of Concrete Structures: Experimental Study, Journal of Wuhan University of Technology-Mater. Sci. Ed, 04/2012, Volume 27, Number 2, pp. 346-352.

[9] Chomette B., Fernandes A., Sinou J.-J., Cracks Detection Using Active Modal Damping and Piezoelectric Components, 2013, Vol.:20 iss:4 pg:619-631.

[10] Kim S. B., Sohn H., Instantaneous reference-free crack detection based on polarization characteristics of piezoelectric materials, 2007 Smart Mater. Struct. 16.

[11] Jeong-Beom I., Fu-Kuo C., Detection and monitoring of hidden fatigue crack growth using a built-in piezoelectric sensor/actuator network: I. Diagnostics, Smart Materials and Structures, 06/2004, Volume 13, Number 3, pp. 609-620.

[12] Cai J., Chen W., Yan W., Lim C., Application of EMI Technique for Crack Detection in Continuous Beams Adhesively Bonded with Multiple Piezoelectric Patches, Mechanics of Advanced Materials and Structures, 01/2008, Volume 15, Number 1, pp. 1-11.

[13] Yu Lingyu, Momeni Sepandarmaz, Godinez Valery, Giurgiutiu Victor, Ziehl Paul, Yu Jianguo, Dual Mode Sensing with Low-Profile Piezoelectric Thin Wafer Sensors for Steel Bridge Crack Detection and Diagnosis, Advances in Civil Engineering, 2012, Volume 2012, pp. 1-10.

[14] Sunyoto S., Bernard Y., Razek A., Design and realization of a linear piezoelectric actuator for orthopaedic applications, Journal of Advanced Science, Vol. 18, Issue: 0, 2006, pp. 162-165.

[15] Hernandez C., Bernard Y., Razek A., A global assessment of piezoelectric actuated micro-pumps, European. Physical Journal Applied Physics, Vol. 51, Issue: 2 (2010) 1-8.

[16] Bernard Y., Razek A., Piezoelectric valve modeling and design, Darmstadt, Germany, 07-08 September 2011, pp.124-131

[17] Hariri H., Bernard Y., Razek A., Locomotion principles for piezoelectric miniature robots, Proceedings on actuator 10, Bremen , DE, 14 June 2010, pp. 1015-1020.

[18] Bernard Y., Hernandez C., Razek A., Radial traveling wave ultrasonic motor design, Actuator14, Breme, DE, 23 June 2014, pp. 663-666, Proceedings of Actuator14.

[19] Tressler James F., Alkoy Sedat, Newnham Robert E., Piezoelectric Sensors and Sensor Materials, Journal of Electroceramics, 12/1998, Volume 2, Number 4, pp. 257-272.

[20] Zimmermann T., Neuburger M., Benkart P., Hernandez-Guillen F.J., Pietzka C., Kunze M., Daumiller I., Dadgar A., Krost A., Kohn E., Piezoelectric GaN sensor structures, IEEE Electron Device Letters, 2006, Volume 27, Number 5, pp. 309-312.

[21] Terada, Jiro, Vibration piezoelectric acceleration sensor, The Journal of the Acoustical Society of America, 2010, Volume 127, Number 3.

[22] Howells Christopher A., Piezoelectric energy harvesting, Energy Conversion and Management, 2009, Volume 50, Number 7, pp. 1847-1850.

[23] Qingyuan Zhu, Yingtai Li, Yuanqin He, Mingjie Guan, Snap-through piezoelectric energy harvesting, Journal of Sound and Vibration, 05/2014, Volume 333, Number 18.

[24] Qingyuan Zhu, Yingtai Li, Yuanqin He, Mingjie Guan, Piezoelectric Energy Harvesting in Automobiles, Ferroelectrics, 01/2014, Volume 467, Number 1.

[25] Hobbs William B., Hu David L., Tree-inspired piezoelectric energy harvesting, Journal of Fluids and Structures, 01/2012, Volume 28.

[26] Corcolle R., Salaün E., Bouillault F., Bernard Y., Richard C., Badel A., Guyomar D., Modeling of a beam structure with piezoelectric materials: introduction to SSD techniques, COMPEL: The International Journal for Computation and Mathematics in Electrical and Electronic Engineering, Vol.27 Issue: 1, (2008) 205-214

[27] de Abreu G.L.C.M., Ribeiro J.F. and Steffen V., Finite element modeling of a plate with localized piezoelectric sensors and actuators, journal of the Braz. Soc. of Mech. Sci. & Eng., Vol. 26, No. 2, (April-June) (2004).

[28] Jalili N., Piezoelectric-Based Vibration Control, From Macro to Micro-Nano Scale Systems, Springer, 2009.

[29] Lin C.C., Huang H.N., Vibration control of beam-plates with bonded piezoelectric sensors and actuators, Journal of computers and structures 73 (1999) 239-248.

[30] Nguyen C.H., Pietrzko S.J., FE analysis of a PZT- actuated adaptive beam with vibration damping using a parallel R-L shunt circuit, journal of finite elements in analysis and design 42, (2006) 1231-1239.

[31] Park C.H., Dynamics modeling of beams with shunted piezoelectric elements, journal of Sound and vibration 268 (2003) 115-129.

[32] Varadan V. V., Closed loop finite element modeling of active/passive damping in structural vibration control, journal of smart materials and structures 5 (1996) 685-694.

[33] Chen J.S., Chen S.H., Wu K.C., Analysis of asymmetric piezoelectric composite beam, DTIP 2007, Stresa, lago Maggiore, Italy, 25-27 April, 2007.

[34] Kayacik O., J.C.B. Jr., Sloss J.M., Adali S., Sadek I. S., Integral equation approach for piezo patch vibration control of beams with various types of damping, Journal of computers and structures 86 (2008) 357-366.

[35] Pons L., Rodríguez H., Rocon E., Fernández J.F., Villegas M., Practical consideration of shear strain correction factor and Rayleigh damping in models of piezoelectric transducers, Journal of Sensors and Actuators A 115 (2004) 202-208.

[36] Corcolle R., Bouillault F., Bernard Y., Modeling of a plate with piezoelectric patches: Damping application, IEEE Transactions on Magnetics vol. MAG 44, no.6 (2008) 798-801.

[37] Liu G.R., Vibration control simulation of laminated composite plates with integrated piezoelectric, Journal of sound and vibration, Vol 220, Issue 5 (1999) 827-846.

[38] Wang S. Y., Dynamic stability analysis of finite element modeling of piezoelectric composite plates, International Journal of Solids and Structures, Vol.41, Issue: 3-4 (2003) 745-764.

[39] Kusculuoglu Z.K., Royston T., Finite element formulation for composite plates with piezoceramic layers for optimal vibration control applications, Journal of Smart Mater. And Struct. 14 (2005) 1139-1153.

[40] Kwon Y. W., Bang H., The Finite Element Method Using MATLAB, Second Edition, CRC Press, 2000.

[41] Liu M., Gorman D. G., Formulation of Rayleigh damping and its extensions, Journal of computers and structures, Vol.57, Issue 2, (1995) 277-285.

[42] Pons L. , Rodríguez H. , Rocon E., Fernández J. F., Villegas M., Practical consideration of shear strain correction factor and Rayleigh damping in models of piezoelectric transducers, Journal of Sensors and Actuators A 115 (2004) 202-208.

[43] Hariri H., Bernard Y., Razek A., Analytical and finite element model for unimorph piezoelectric actuator: Actuator design, Proceedings of Piezo2011, sestriere, 27 February 2011, pp. 71-75

[44] Wang Q. M., Cross L. E., Performance analysis of piezoelectric cantilever bending actuators, Journal of Ferroelectrics, Vol. 215 (1998) 187-213.